Ocean Dynamics manuscript No.
(will be inserted by the editor)

Benchmarking Tsunami Models using the December 2004 Indian Ocean Tsunami and its Impact at Patong City, Thailand

J. D. Jakeman · O. Nielsen · K. Van Putten · R. Mleczko · D. Burbidge · N. Horspool

the date of receipt and acceptance should be inserted later

Abstract This paper proposes a new benchmark for tsunami model validation. The benchmark is based upon the 2004 Indian Ocean tsunami, which affords a uniquely large amount of observational data for events of this kind. The proposed benchmark is intended to aid validation of tsunami inundation modelling, which is the most important stage of tsunami evolution. However, individual tests are presented to facilitate model evaluation for the generation and propagation phases as well. Specifically, we use geodetic measurements of the Sumatra–Andaman earthquake to validate the tsunami source, altimetry data from the JASON satellite to test open ocean propagation, eye-witness accounts to assess near shore propagation and a detailed inundation survey of Patong City, Thailand to compare model and observed inundation. Furthermore we utilise this benchmark to further validate the modelling methodology used by Geoscience Australia to simulate the tsunami inundation. Important buildings and other structures were incorporated into the underlying computational mesh and are shown to have a large influence on inundation extent.

Keywords Tsunami · modelling · validation and verification · benchmark

Contents

J. D. Jakeman
The Australian National University, Canberra, AUSTRALIA E-mail: john.jakeman@anu.edu.au

O. Nielsen · K. Van Putten · R. Mleczko · D. Burbidge · N. Horspool
Geoscience Australia, Canberra, AUSTRALIA

1 Introduction

Tsunami is a potential hazard to coastal communities all over the world. A number of recent large events have increased community and scientific awareness of the need for effective detection, forecasting, and emergency preparedness. Probabilistic, geophysical and hydrodynamic models are required to predict the location and likelihood of an event, the initial sea floor deformation and subsequent propagation and inundation of the tsunami. Engineering, economic and social vulnerability models can then be used to estimate the impact of the event as well as the effectiveness of hazard mitigation procedures. In this paper, we focus on modelling of the physical processes only.

Various approaches are currently used to assess the potential tsunami inundation of coastal communities. These methods differ in both the formulation used to describe the evolution of the tsunami and the numerical methods used to solve the governing equations. The structure of these models ranges from data-driven neural networks [20] to non-linear three-dimensional mechanical models [34]. These models are typically used to predict quantities such as arrival times, wave speeds and heights, as well as inundation extents that can be used to develop efficient hazard mitigation plans. Physics based models combine observed seismic, geodetic and sometimes tide gauge data to provide estimates of initial sea floor and ocean surface deformation. The shallow water wave equations [9], linearised shallow water wave equations [14], and Boussinesq-type equations [32] are frequently used to simulate tsunami propagation and inundation.

Inaccuracies in model prediction can result in inappropriate evacuation plans, town zoning and land use planning, which ultimately may result in loss of life and infrastructure. Consequently tsunami models must undergo sufficient end-to-end testing to increase scientific and community confidence in the model predictions.

Complete confidence in a model of a physical system cannot be established. One can only hope to state under what conditions and to what extent the model hypothesis holds true. Specifically, the utility of a model can be assessed through a process of verification and validation. Verification assesses the accuracy of the numerical method used to solve the governing equations and validation is used to investigate whether the model adequately represents the physical system [5]. Together these processes can be used to establish the likelihood that a model represents a legitimate hypothesis.

The sources of data used to validate and verify a model can be separated into three main categories: analytical solutions, scale experiments and field measurements. Analytical solutions, of the governing equations of a model, if available, provide the best means of verifying any numerical model. However, analytical solutions are frequently limited to a small set of idealised examples that do not completely capture the more complex behaviour of 'real' events. Scale experiments, typically in the form of wave-tank experiments, provide a much more realistic source of data that better captures the complex dynamics of flows such as those generated by a tsunami, whilst allowing control of the event and much easier and accurate measurement of the tsunami properties. Comparison of numerical predictions with field data provides the most stringent test. The use of field data increases the generality and significance of conclusions made regarding model utility [5].

Currently, the extent of tsunami-related field data is limited. The cost of tsunami monitoring programs and the rarity of events as well as bathymetry and topography surveys prohibits the collection of data in many of the regions in which tsunamis pose the greatest threat. The resulting lack of data has limited the number of field data sets available to validate tsunami models.

Synolakis et al [24] have developed a set of standards, criteria and procedures for evaluating numerical models of tsunami. They propose a number of analytical solutions to help identify the validity of a model, and five scale comparisons (wave-tank benchmarks) and two field events to assess model veracity.

The first field data benchmark introduced in [24] compares model results against observed data from the Hokkaido-Nansei-Oki tsunami that occurred around Okushiri Island, Japan on the 12 July 1993. This tsunami provides an example of extreme run-up generated from reflections and constructive interference resulting from local topography and bathymetry. The benchmark consists of two tide gauge records and numerous spatially-distributed point sites at which modelled maximum run-up elevations can be compared. The second benchmark is based upon the Rat Islands tsunami that occurred off the coast of Alaska on the 17 November 2003. The Rat Island tsunami provides a good test for real-time forecasting models since the tsunami was recorded at three tsunameters. The test requires matching the tsunami propagation model output with the tsunameter recordings to constrain the tsunami source model, and then using it to reproduce the tide gauge record at Hilo, Hawaii.

In this paper we develop a field data benchmark to be used in conjunction with the other tests proposed by Synolakis et al [24] to validate and verify tsunami models. The benchmark proposed here allows evaluation of model components during three distinct stages tsunami evolution, namely generation, propagation and inundation. It consists of geodetic measurements of the Sumatra–Andaman earthquake that are used to validate the description of the tsunami source, altimetry data from the JASON satellite to test open ocean propagation, eye-witness accounts to assess near shore propagation, and a detailed inundation survey of Patong City, Thailand to compare model and observed inundation. A description of the data required to construct the benchmark is given in Section 2.

Previous model field evaluations [31, 12] and benchmarks [24] have focused on reproducing inundation at point sites, which are often sparsely distributed. The stakeholders in any tsunami study, such as emergency planners are generally more interested in more detailed localised studies of tsunami impacts on populated areas. Informed and defensible decisions must be based upon detailed simulations that predict local inundation extents. Ideally validation studies should be tailored accordingly.

Unlike the existing field benchmarks, the proposed test facilitates localised and highly detailed spatially distributed assessment of modelled inundation. To the authors knowledge it is also the first benchmark to assess model inundation influenced by numerous human made structures. Eye-witness videos have also been considered to allow the qualitative assessment of onshore flow patterns.

An associated aim of this paper is to illustrate the use of this new benchmark to validate the three step modelling methodology employed by Geoscience Australia to model tsunami inundation. A description of the model components is provided in Section 3 and the validation results are given in Section 4.

The numerical models used to simulate tsunami impact are computationally intensive and high resolution models of the entire evolution process will often require a number of days to complete. Consequently, the uncertainty in model predictions is difficult to quantify as it would require a very large number of simulations. However, model uncertainty should not be ignored. Section 5 provides a simple analysis that can be used to investigate the sensitivity of model predictions to a number of key model parameters.

2 Data

The sheer magnitude of the 2004 Sumatra-Andaman earthquake and the devastation caused by the subsequent tsunami have generated much scientific interest. As a result an unusually large amount of post seismic data has been collected and documented. Data sets from seismometers, tide gauges, GPS surveys, satellite overpasses, subsequent coastal field surveys of run-up and flooding, and measurements of coseismic displacements as well as bathymetry from ship-based expeditions and high quality topographic data, have now been made available.

In this section we present the corresponding data necessary to implement the proposed benchmark. Here we note that the overwhelming focus of tsunami modelling is the prediction of inundation extent. The "fit" of observed and modelled runup should have the greatest influence on conclusions regarding model validity. In fact for non-physics based models it may not be possible to validate the generation and propagation phases of tsunami evolution. However, for physics-based models evaluation of the model during the generation and propagation phases is still useful. If a model is physics-based one should ensure that all physics are being modelled accurately. Moreover, evaluation of all three stages of tsunami evolution can help identify the cause of any discrepancies between modelled and observed inundation. Consequently, in this section we present data not only to facilitate validation of inundation extent but to also aid the assessment of tsunami generation and propagation.

2.1 Generation

All tsunami are generated from an initial disturbance of the ocean which develops into a low frequency wave that propagates outwards from the source. The initial deformation of the water surface is most commonly caused by coseismic displacement of the sea floor, but submarine mass failures, landslides, volcanoes or asteroids can also cause tsunami. In this section we detail the information used in this study to validate models of the sea floor deformation generated by the 2004 Sumatra–Andaman earthquake.

The 2004 Sumatra–Andaman tsunami was generated by a coseismic displacement of the sea floor resulting from one of the largest earthquakes on record. The mega-thrust earthquake started on the 26 December 2004 at 0h58'53" UTC (or just before 8 am local time) approximately 70 km offshore of North Sumatra (`http://earthquake.usgs.gov/eqcenter/eqinthenews/2004/usslav`). The rupture propagated 1000-1300 km along the Sumatra-Andaman trench to the north at a rate of 2.5-3 km.s^{-1} and lasted approximately 8-10 minutes [1]. Estimates of the moment magnitude of this event range from about 9.1 to 9.3 M_w [7,23].

The unusually large surface deformation caused by this earthquake means that there were a range of different geodetic measurements of the surface deformation available. These include field measurements of uplifted or subsided coral heads, continuous or campaign GPS measurements and remote sensing measurements of uplift or subsidence (see [7] and references therein). Here we use the the near-field estimates of vertical deformation in northwestern Sumatra and the Nicobar-Andaman islands collated by [7] to assess whether our crustal deformation model of the 2004 Sumatra–Andaman earthquake is producing reasonable results. Note that the geodetic data used here is a combination of the vertical deformation that happened in the $\sim$10 minutes of the earthquake plus the deformation that followed in the days following the earthquake before each particular measurement was actually made

(typically of the order of days). Therefore some of the observations may not contain the purely co-seismic deformation but could include some post-seismic deformation as well [7].

2.2 Propagation

Once generated, a tsunami will propagate outwards from the source until it encounters the shoreline bordering coastal regions. This part of the tsunami evolution is referred to as the propagation stage. The height and speed of the tsunami are dependent on the local bathymetry in the regions through which the wave travels and the characteristics of the initial wave. This section details the bathymetry data needed to model the tsunami propagation and the satellite altimetry transects used here to validate open ocean tsunami models.

2.2.1 Bathymetry Data

The bathymetry data used in this study were derived from the following sources:

- a two arc minute data grid covering the Bay of Bengal, DBDB2, obtained from US Naval Research Labs (`http://www7320.nrlssc.navy.mil/DBDB2_WWW`);
- a three arc second data grid obtained directly from NOAA covering the whole of the Andaman Sea based on the Smith & Sandwell two minute dataset (`http://topex.ucsd.edu/WWW_html/srtm30_plus.html`), coastline constrained using SRTM data (`http://srtm.csi.cgiar.org`) as well as Thai Navy charts no. 45 and no. 362; and
- Thai Navy chart no. 358 providing depth soundings inside Patong Bay.

These data sets were used to produce four nested grids as shown in Figure 1. The nested approach was chosen to match model resolution requirements according to the principle that shallow water flows are more sensitive to variations in elevation data than deep water flows. Consequently, the elevation data in shallow waters and on-shore need to be better resolved than elevation data further off-shore. The four nested grids were derived as follows:

- **27 arc second grid** obtained by interpolating the two minute DBDB2 grid. This is the coarsest grid used in the simulations.
- **9 arc second grid** generated by sub-sampling the three second arc grid from NOAA.
- **3 arc second grid** formed as a subset of the three second grid from NOAA.
- **1 arc second grid** created by digitising Thai Navy bathymetry chart no. 358 followed by a gridding procedure as described below. This grid is the smallest and covers the Patong Bay area and immediately adjacent regions. The digitised points and contour lines from this chart are shown in Figure 2.

The gridding process for the finest grid was performed using INTREPID, a commercial geophysical processing package developed by Intrepid Geophysics[1]. Any points that deviated from the general trend near the boundary were deleted through a quality control process. The sub-sampling of larger grids was performed by using RESAMPLE, a Generic Mapping Tools (GMT) program [33].

[1] See `http://www.intrepid-geophysics.com/ig/manuals/english/gridding.pdf` for details on the Intrepid gridding scheme.

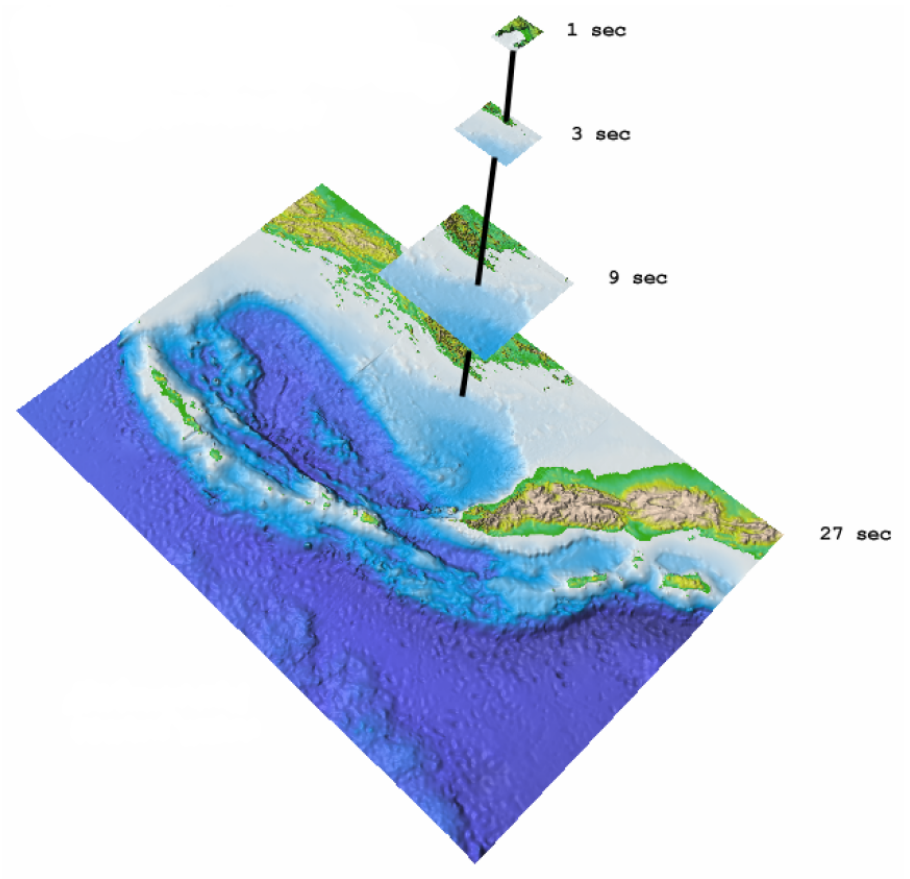

Fig. 1 Nested elevation grids of the Andaman Sea with highest resolution at and around Patong Bay.

2.2.2 JASON Satellite Altimetry

During the 2004 Sumatra-Andaman event, the JASON satellite tracked from north to south and over the equator at 02:55 UTC nearly two hours after the earthquake [10]. The satellite recorded the sea level anomaly compared to the average sea level from its previous five passes over the same region in the 20-30 days prior. This data was used to validate the propagation stage in Section 4.2.

2.3 Inundation

Inundation is the final stage of the evolution of a tsunami and refers to the run-up of tsunami onto land. This process is typically the most difficult of the three stages to model due to thin layers of water flowing rapidly over dry land. Aside from requiring robust solvers which can simulate such complex flow patterns, this part of the modelling process also requires high resolution and quality elevation data which is often not available. In the case of model validation, high quality field measurements are also required. For the proposed benchmark

a high resolution topography data set (in the form of GIS contour lines) and a tsunami inundation survey map from the Coordinating Committee for Geoscience Programmes in East and Southeast Asia (CCOP) [26] was obtained to validate model inundation. In this section we also present eye-witness accounts which can be used to qualitatively validate tsunami inundation.

2.3.1 Topography Data

A 1 second grid comprising the onshore topography and the nearshore bathymetry for Patong Beach was created from the Thai Navy charts (described in Section 2.2.1) and from 1 m and 10 m elevation contours provided by the CCOP. The 1 second terrain model for the community is shown in Figure 2.

To provide increased resolution for the surveyed area, two 1/3 second grids were created: One for the saddle point covering Merlin and Tri Trang Beaches (separate survey patch to the left in Figure 3) and one for Patong City and its immediate shore area (main surveyed area in Figure 3). These grids were based on the same data used for the 1 second data grid. The Patong City grid was further modified based on satellite imagery to include the river and lakes towards the south of Patong City which were not part of the provided elevation data. In the absence of data, the depth of the river and lake system was set uniformly to a depth of 1 m.

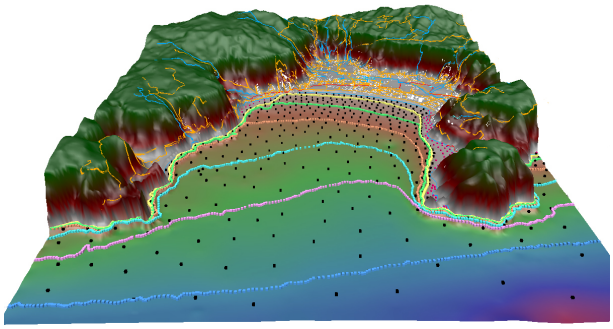

Fig. 2 3D view of the elevation data set used for the nearshore propagation and inundation in Patong City showing digitised data points and contours as well as rivers and roads draped over the data model.

2.3.2 Buildings and Other Structures

Human-made buildings and structures can significantly affect tsunami inundation. The footprint and number of floors of the buildings in Patong City were extracted from the data provided by CCOP. The heights of these buildings were estimated assuming that each floor has a height of 3 m and the resulting profiles were added to the topographic dataset. The resulting elevation model and its interaction with one of the tsunami waves can be seen in Figure 11 in Section 4.3.

2.3.3 Inundation Survey

Tsunami run-up in built-up areas can be the cause of large financial and human losses, yet run-up data that can be used to validate model run-up predictions is scarce because such events are relatively infrequent. Of the two field benchmarks proposed in [24], only the Okushiri benchmark facilitates comparison between modelled and observed run-up. One of the major strengths of the benchmark proposed here is that modelled run-up can be compared to an inundation survey which maps the maximum run-up along an entire coastline rather than at a series of discrete sites. The survey map is shown in Figure 3 and plots the maximum run-up of the 2004 Indian Ocean tsunami in Patong City. Refer to Szczucinski et al [26] for further details.

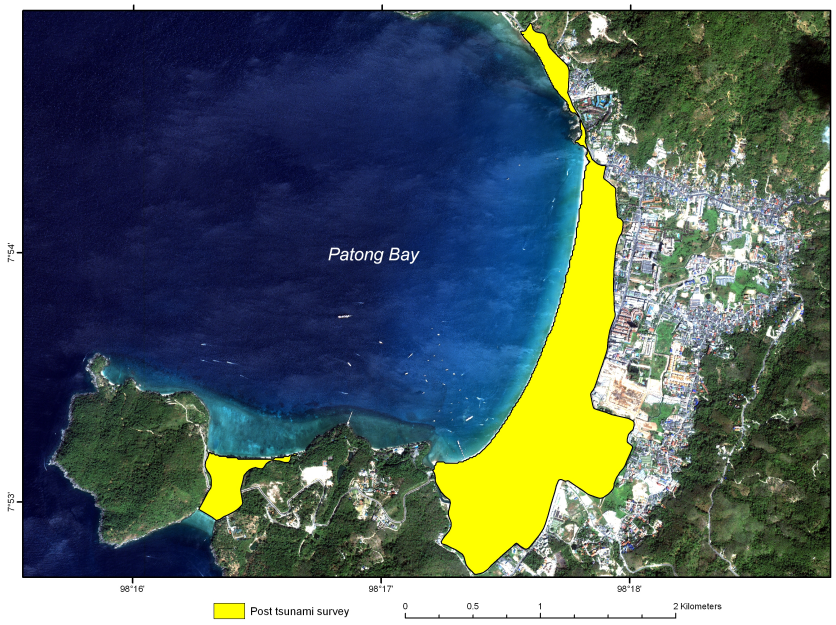

Fig. 3 Tsunami survey mapping the maximum observed inundation at Patong City, courtesy of the CCOP [26].

2.3.4 Eyewitness Accounts

Eyewitness accounts detailed in [17] report that many people at Patong Beach observed an initial retreat (trough or draw down) of the shoreline of more than 100 m followed a few minutes later by a strong wave (crest). Another less powerful wave arrived another five or ten minutes later. Eyewitness statements place the arrival time of the first wave between 9:55 am and 10:05 am local time or about two hours after the source rupture.

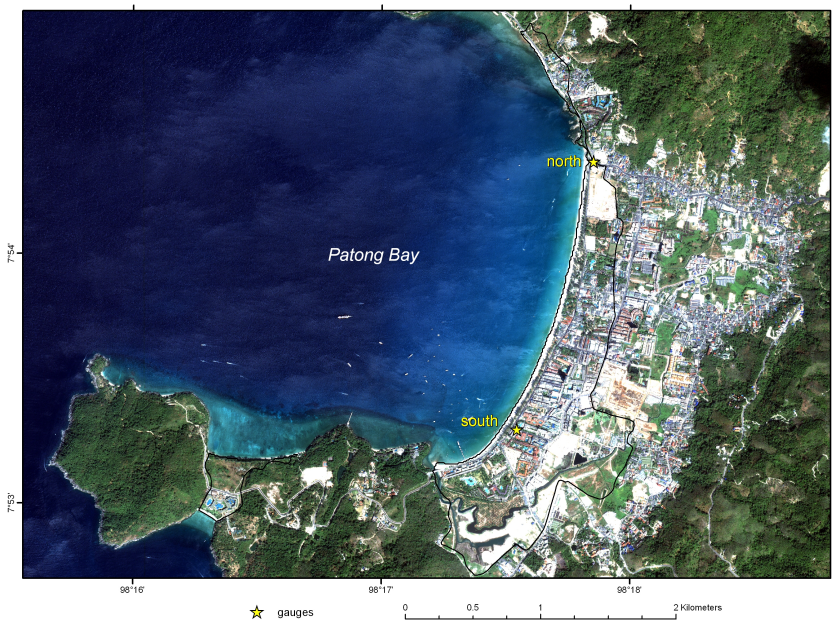

Fig. 4 Location of time series extracted from the model output.

Two videos were sourced[2] which include footage of the tsunami in Patong City on the day of the 2004 Indian Ocean tsunami. Both videos show an already inundated street. They also show what is to be assumed as the second and third waves approaching and further flooding of the buildings and street. The first video is in the very north, filmed from what is believed to be the roof of the Novotel Hotel marked "north" in Figure 4. The second video is in the very south, filmed from the second story of a building next door to the Comfort Resort near the corner of Ruam Chai St and Thaweewong Road. This location is marked "south" in Figure 4. Figure 5 shows stills from this video. Both videos were used to estimate flow speeds and inundation depths over time.

Flow rates were estimated using landmarks found in both videos and were found to be in the range of 5 to 7 m/s ($\pm$2 m/s) in the north and 0.5 to 2 m/s ($\pm$1 m/s) in the south[3]. Water depths could also be estimated from the videos by the level at which water rose up the sides of buildings such as shops. Our estimates are in the order of 1.5 to 2.0 m ($\pm$0.5 m estimated error bounds). Fritz [8] performed a detailed analysis of video frames taken around Banda Aceh and arrived at flow speeds in the range of 2 to 5 m/s.

[2] The footage is widely available and can, for example, be obtained from `http://www.archive.org/download/patong_bavarian/patong_bavaria.wmv` (Comfort Resort) and `http://www.archive.org/download/tsunami_patong_beach/tsunami_patong_beach.wmv` (Novotel).

[3] These error bounds were estimated from uncertainty in aligning the debris with building boundaries in the videos.

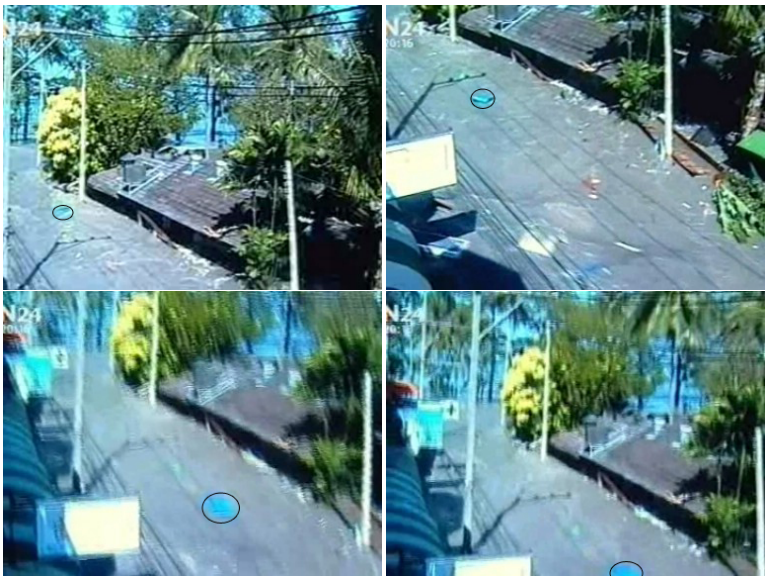

Fig. 5 Four frames from a video where flow rate could be estimated, circle indicates tracked debris, from top left: 0.0 s, 5.0 s, 7.1 s, 7.6 s.

2.4 Validation Check-List

The data described in this section can be used to construct a benchmark to validate tsunami models. In particular we propose that a legitimate tsunami model should reproduce the following behaviour:

- the inundation survey map in Patong City (Figure 3),
- a leading depression followed by two distinct crests of decreasing magnitude at the beach,
- predict the water depths and flow speeds, at the locations of the eye-witness videos, that fall within the bounds obtained from the videos,
- the JASON satellite altimetry sea surface anomalies (see Section 2.2.2), and
- the vertical deformation observed in north-western Sumatra and along the Nicobar–Andaman islands (see Section 2.1).

Ideally, the model should also be compared to measured time series of wave heights and flow speeds but the authors are not aware of the availability of such data near Patong Bay.

3 Modelling the Event

Numerous models are currently used to simulate tsunami generation, propagation and inundation. These range in solving different equations and employing different methodologies with some examples being [29,21,34]. Here we introduce the modelling methodology employed by Geoscience Australia to illustrate the utility of the proposed benchmark. The methodology used by Geoscience Australia has three distinct components. Firstly an appropriate model is used to approximate the initial sea surface deformation. This model is chosen

according to the cause of the intial disturbance. The resulting wave is propagated using the URSGA model (see Section 3.2.1) in the deep ocean until the wave reaches shallow water, typically the 100 m depth contour. The ocean surface profile along this contour is used as a time varying boundary condition for the ANUGA model (see Section 3.3.1) which simulates the propagation of the tsunami within the shallow water and the subsequent inundation of the land. This three part methodology roughly follows the three stages of tsunami evolution. The components used to model each stage of evolution are described in more detail below.

3.1 Generation

There are various approaches to modelling the expected crustal deformation from an earthquake. Most approaches model the earthquake as a dislocation in a linear elastic medium. Here we use the method of Wang et al [30]. In order to calculate the crustal deformation a model that describes the variation in elastic properties with depth and a slip model of the earthquake to describe the dislocation is required. The elastic parameters used for this study are the same as those in Table 2 of Burbidge et al [6]. For the slip model, there are many possible models for the 2004 Andaman–Sumatran earthquake to select from [7,3,2,11,12]. Some are determined from various geological surveys of the site. Others solve an inverse problem that calibrates the source based upon the tsunami wave signal, the seismic signal and/or even the run-up. The source parameters used here to simulate the 2004 Indian Ocean tsunami were taken from the slip model G-M9.15 of Chlieh et al [7]. This model was created by inversion of wide range of geodetic and seismic data. The slip model consists of 686 20 km x 20 km subsegments each with a different slip, strike and dip angle. The dip subfaults range from 17.5° in the north and 12° in the south. Refer to Chlieh et al [7] for a detailed discussion of this model and its derivation.

3.2 Open water propagation

The URSGA model described below was used to simulate the propagation of the 2004 Indian Ocean tsunami across the open ocean, based on a discrete representation of the initial deformation of the sea floor, as described in Section 3.1. For the models shown here, the uplift is assumed to be instantaneous and creates an initial displacement of the ocean surface of the same size and amplitude as the co-seismic sea floor deformation. URSGA is well suited to modelling propagation over large domains and is used to propagate the tsunami until it reaches shallow water, typically the 100 m depth contour.

3.2.1 URSGA

URSGA is a hydrodynamic code that models the propagation of the tsunami in deep water using a finite difference method on a staggered grid. It solves the depth integrated linear or nonlinear shallow water equations in spherical co-ordinates with friction and Coriolis terms. The code is based on Satake [21] with significant modifications made by the URS corporation, Thio et al [27] and Geoscience Australia, Burbidge et al [6]. The tsunami was propagated via the nested grid system described in Section 2.2 where the coarse grids were used in the open ocean and the finest resolution grid was employed in the region closest to Patong Bay. URSGA is not publicly available.

3.3 Shallow water propagation and inundation

The utility of the URSGA model decreases with water depth unless an intricate sequence of nested grids is employed. In comparison ANUGA, described below, is designed to produce robust and accurate predictions of inundation, but is less suitable for earthquake source modelling and large study areas because it is based on projected spatial coordinates. Consequently, the Geoscience Australia tsunami modelling methodology is based on a hybrid approach using models like URSGA for tsunami propagation up to an offshore depth contour, typically 100 m. The wave signal and the velocity field is then used as a time varying boundary condition for the ANUGA inundation simulation.

3.3.1 ANUGA

ANUGA is a free and open source hydrodynamic inundation tool that solves the conserved form of the depth-integrated nonlinear shallow water wave equations using a finite-volume scheme on an unstructured triangular mesh. The scheme, first presented by Zoppou and Roberts [35], is a high-resolution Godunov-type method that uses the rotational invariance property of the shallow water equations to transform the two-dimensional problem into local one-dimensional problems. These local Riemann problems are then solved using the semi-discrete central-upwind scheme of Kurganov et al [13] for solving one-dimensional conservation equations. The numerical scheme is presented in detail in Roberts and Zoppou [36, 19] and Nielsen et al [16]. An important capability of the finite-volume scheme is that discontinuities in all conserved quantities are allowed at every edge in the mesh. This means that the tool is well suited to adequately resolving hydraulic jumps, transcritical flows and the process of wetting and drying. Consequently, ANUGA is suitable for simulating water flow onto a beach or dry land and around structures such as buildings. ANUGA has been validated against the wave tank simulation of the 1993 Okushiri Island tsunami [16, 18] and dam break experiments [4]. More information on ANUGA and how to obtain it are available from `https://datamining.anu.edu.au/anuga`.

4 Results

This section presents a validation of the modelling practice of Geoscience Australia against the new proposed benchmarks. The criteria outlined in Section 2.4 are addressed.

4.1 Generation

The location and magnitude of the sea floor displacement associated with the 2004 Sumatra–Andaman tsunami calculated from the G-M9.15 model of [7] is shown in Figure 6. As can be seen, the source model detailed in Section 3.1 produces a crustal deformation that matches the vertical displacements in the Nicobar-Andaman islands and Sumatra very well. Uplifted regions are close to the fault and subsided regions are further away. The crosses on Figure 6 show estimates of the pivot line from the remote sensing data [7] and they follow the predicted pivot line quite accurately. The average difference between the observed motion and the predicted motion (including the pivot line points) is only 0.06 m, well below the typical error of the observations of between 0.25 and 1.0 m.

The excellence of the fit is not surprising, since the original slip model was chosen by [7] to fit the motion and seismic data well. Consequently, the replication of the generation data has limited meaning for the model structure presented in Section 3. However, for uncalibrated source models or source models calibrated on other data this test of generation would be more meaningful.

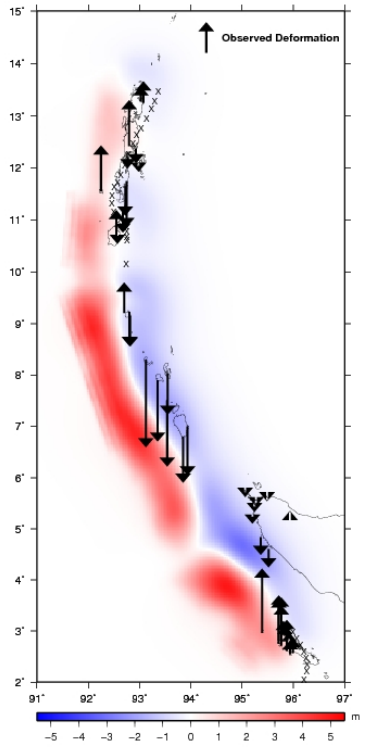

Fig. 6 Location and magnitude of the vertical component of the sea floor displacement associated with the 2004 Indian Ocean tsunami based on the slip model, G-M9.15 compared with observed deformation (arrows). The black arrows which point up show areas observed to uplift during and immediately after the earthquake; those pointing down are locations which subsided. The length of the arrow increases with the magnitude of the deformation. The arrow length corresponding to 1 m of deformation is shown in the top right hand corner of the figure. The cross marks show the location of the pivot line (the region between the uplift and subsided region where the uplift is zero) derived from remote sensing of where there were no changes in the amount of reef or land exposure before and after the earthquake [15]. All the observational data are from the dataset collated by [7].

4.2 Propagation

The deformation results described in Section 3.1 were used to provide a profile of the initial ocean surface displacement. This wave was used as an initial condition for URSGA and was propagated throughout the Bay of Bengal. The rectangular computational domain of the largest grid extended from 90° to 100° East and 0° to 15° North and contained 1335×1996 finite difference points. Inside this grid, a nested sequence of grids was used. The grid resolution of the nested grids went from 27 arc seconds in the coarsest grid, down to nine arc seconds in the second grid and three arc seconds in the third grid. The computational domain is shown in Figure 7.

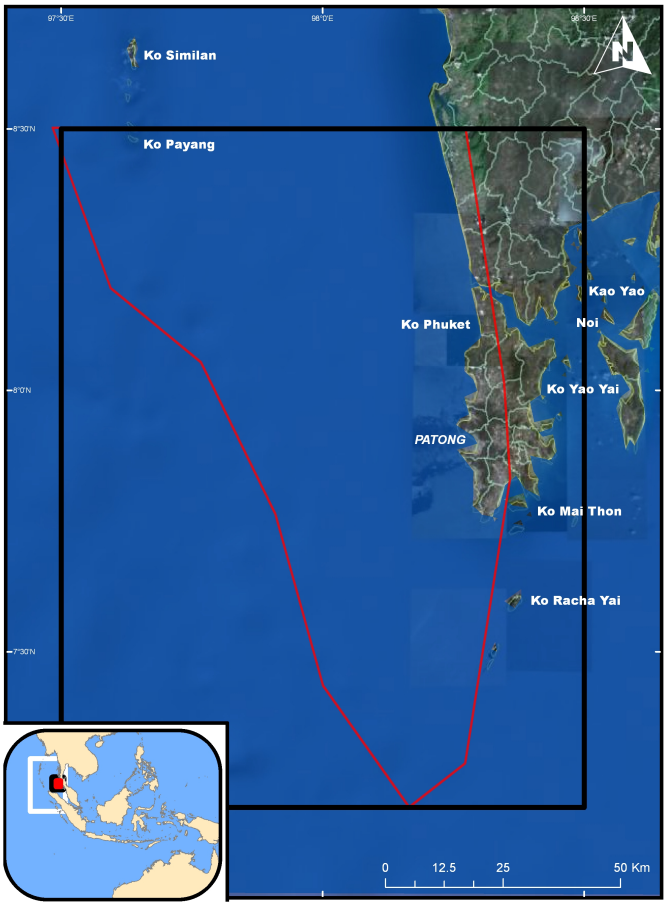

Fig. 7 Computational domain of the URSGA simulation (inset: white and black squares and main: black square) and the ANUGA simulation (main and inset: red polygon).

Figure 8 provides a comparison of the URSGA-predicted sea surface elevation with the JASON satellite altimetry data. The URSGA model replicates the amplitude and timing of the the wave observed at 2.5° South, but underestimates the amplitude of the wave further to the south at 4° South. In the model, the southern most of these two waves appears only as a small bump in the cross section of the model (shown in Figure 8) instead of being a distinct peak as can be seen in the satellite data. Also note that the URSGA model prediction of the ocean surface elevation becomes out of phase with the JASON data at 3° to 7° North latitude. Chlieh et al [7] also observed these misfits and suggest it is caused by a reflected wave from the Aceh Peninsula that is not resolved in the model due to insufficient resolution of the computational mesh and bathymetry data. This is also a limitation of the model presented here which could be improved by nesting grids near Aceh.

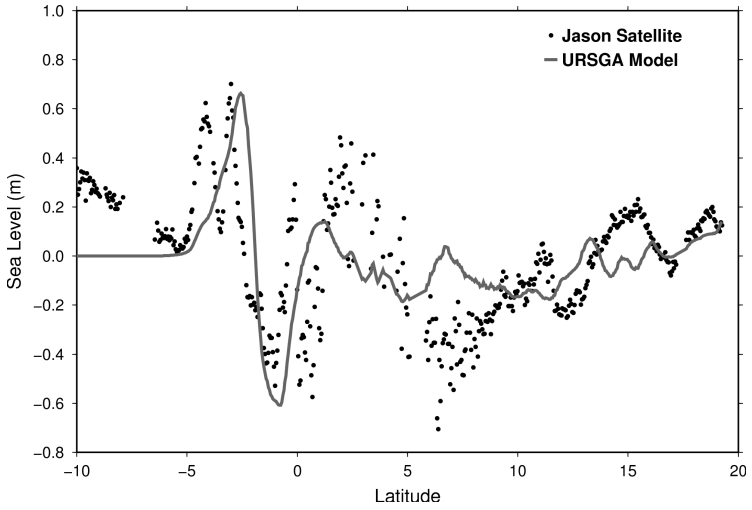

Fig. 8 Comparison of the URSGA-predicted surface elevation with the JASON satellite altimetry data. The URSGA wave heights have been corrected for the time the satellite passed overhead compared to JASON sea level anomaly.

After propagating the tsunami in the open ocean using URSGA, the approximated ocean surface elevation and horizontal flow speeds were extracted and used to construct a boundary condition for the ANUGA model. The interface between the URSGA and ANUGA models was chosen to roughly follow the 100 m depth contour along the west coast of Phuket Island. Data from the three second grid which is approximately 30 m apart was decimated to match the resolution chosen in ANUGA. The computational domain is shown in Figure 7.

The domain was discretised into 386,338 triangles. The resolution of the grid was increased in regions inside the bay and on-shore to efficiently increase the simulation accuracy for the impact area. The grid resolution ranged between a maximum triangle area of 1×10^5 m^2 (corresponding to approximately 440 m between mesh nodes) near the western ocean boundary (roughly following the 100 m depth contour) to 20 m^2 (corresponding to approximately 6 m between mesh nodes) in the small regions surrounding the inundation region in Patong City and intertidal zone. The coarse resolution was chosen to balance accuracy with computational costs while the fine resolution was chosen to match the available

resolution of topographic data and building data in Patong City. Figure 9 shows a section of the mesh covering the southern part of the City.

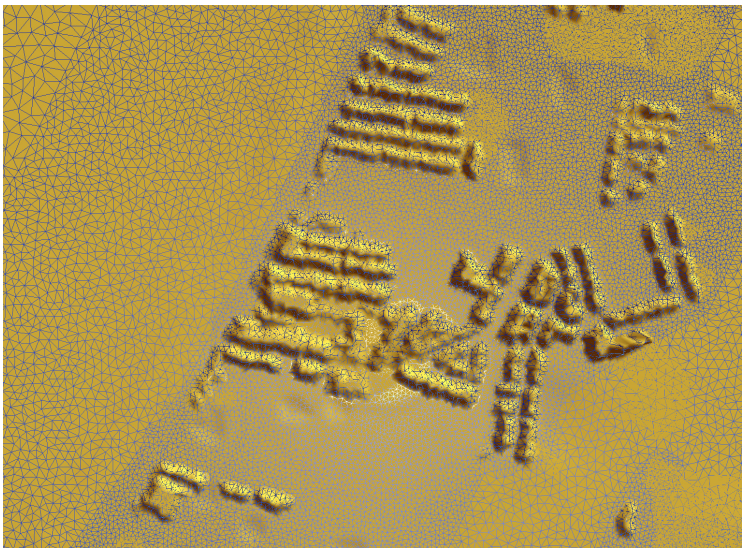

Fig. 9 Section of the mesh used by ANUGA to simulate the tsunami inundation. The finest mesh resolution is approximately 6 m between nodes which is sufficient to resolve individual buildings affecting the flows.

Due to a lack of available roughness data, Manning friction was set to a constant throughout the computational domain. For the reference simulation, a Manning's coefficient of 0.01 was chosen to represent a small resistance to the water flow. See Section 5.1 for details on model sensitivity to this parameter.

As the URSGA model in this study was used to compute the incident wave along the 100 m contour line only, there is no such information available at each side of the ANUGA domain towards the south and the north. Instead, a transmissive boundary condition was chosen for these segments, effectively replicating the time dependent wave height present just inside the computational domain. The velocity field on these boundaries was kept at zero during the simulation. Other choices include applying the mean tide value as a Dirichlet boundary condition. Experiments as well as the result of the verification reported here showed that this approach tends to underestimate the tsunami impact due to the tempering of the wave near the side boundaries, whereas the transmissive boundary condition robustly preserves the wave.

During the ANUGA simulation the tide was kept constant in the offshore region at 0.80 m. This value was chosen to correspond to the tidal height specified by the Thai Navy tide charts (`http://www.navy.mi.th/hydro/`) at the time the tsunami arrived at Patong Bay. Although the tsunami propagated for approximately three hours before it reached Patong Bay, the period of time during which the wave propagated through the ANUGA domain is much smaller by of the order of two hours. Consequently the assumption of constant tide height is reasonable. The initial water level for the river was set to 0 m.

4.3 Inundation

The ANUGA simulation described in the previous section and used to model shallow water propagation also predicts inundation. Maximum onshore inundation depth was computed from the inundation model and used to generate a measure of the inundated area. Figure 10 (left) shows very good agreement between the measured and simulated inundation. However, these results are dependent on the classification used to determine whether a region in the numerical simulation was inundated. In Figure 10 (left) a point in the computational domain was deemed inundated if at some point in time it was covered by at least 1 cm of water. The precision of the inundation boundary generated by the on-site survey is most likely less than this as it was determined by observing water marks and other signs left by the receding waters. Consequently, the measurement error along the inundation boundary of the survey is likely to vary significantly and somewhat unpredictably. An inundation threshold of 10 cm therefore was selected for inundation extents reported in this paper to reflect the more likely accuracy of the survey, and subsequently facilitate a more appropriate comparison between the modelled and observed inundation area. Figure 10 (right) shows the simulated inundation using a larger threshold of 10 cm and Figure 11 shows a screenshot from the inundation model. An animation of this simulation is available on the ANUGA website at `https://datamining.anu.edu.au/anuga` or directly from `http://tinyurl.com/patong2004`.

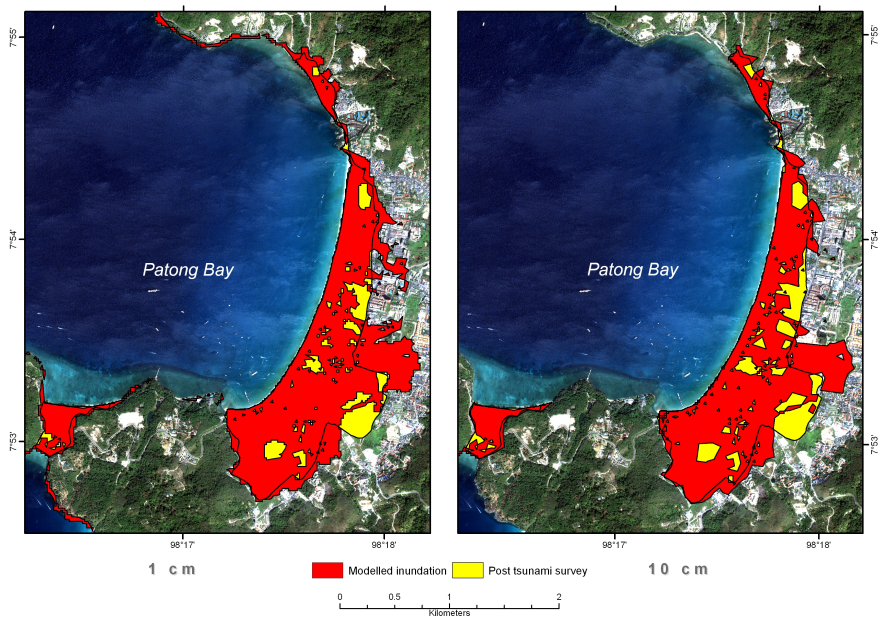

Fig. 10 Simulated inundation versus observed inundation using an inundation threshold of 1 cm (left) and 10 cm (right).

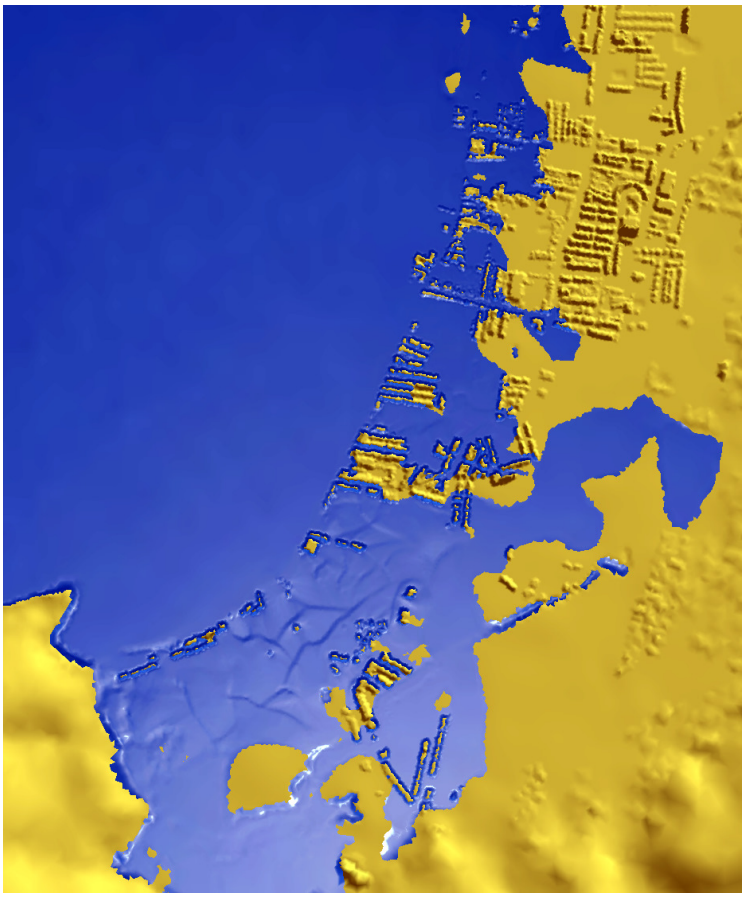

Fig. 11 Screenshot of the ANUGA simulation of the inundation at Patong City at local time 10:53 about one hour after the arrival of the first wave.

4.3.1 Comparison to survey

To quantify the agreement between the observed and simulated inundation we introduce the measure

$$\rho_{in} = \frac{A(I_m \cap I_o)}{A(I_o)} \tag{1}$$

representing the ratio of the area of the observed inundation region I_o and the area of the observed inundation region captured by the model I_m. Another useful measure is the fraction of the modelled inundation area that falls outside the observed inundation area given by the formula

$$\rho_{out} = \frac{A(I_m \setminus (I_m \cap I_o))}{A(I_o)} \tag{2}$$

These values for the two aforementioned simulations are given in Table 2 along with results from the sensitivity analysis in Section 5. High values of both ρ_{in} and ρ_{out} indicate that the model overestimates the impact whereas low values of both quantities would indicate an

underestimation. A high value of ρ_{in} combined with a low value of ρ_{out} indicates a good model prediction of the survey.

Discrepancies between the survey data and the modelled inundation arise from errors and uncertainties in both the field surveys and the models. The former include measurement errors in the GPS survey recordings and missing data in the field survey data itself. The latter include unknown distribution of surface roughness, uncertainties in the parameterisation of the source model, discretisation errors, effect of humans structures on flow, as well as uncertainties in the elevation data including effects of erosion and deposition by the tsunami event. The impacts of some of the model uncertainties are as investigated in Section 5.

4.3.2 Reproducibility of inundation results

As one aim of this paper is to provide a new benchmark for tsunami inundation modelling we have made the datasets available available on SOURCEFORGE in the ANUGA project (`http://sourceforge.net/projects/anuga`) under the directory `validation_data/patong-1.0`. At the time of writing a direct link is `http://tinyurl.com/patong2004-data`.

To reproduce the inundation modelling results using this data, the reader will need to run the validation scripts (`anuga_validation/automated_validation_tests/patong_beach_validation`) which are part of the ANUGA distribution also available from SOURCEFORGE `http://sourceforge.net/projects/anuga`.

4.4 Eye-witness accounts

4.4.1 Arrival time

The arrival time of the first wave took place between 9:55 and 10:05 as described in Section 2.3.4. The modelled arrival time at the beach is around 10:02 as can be verified from the animation provided in Section 4.3 or from Figure 12 below. Subsequent waves of variable magnitude appear over the next two hours approximately 20-30 minutes apart. The first arrival and overall dynamic behaviour is therefore reasonably consistent with the eye-witness accounts.

4.4.2 Observed wave dynamics

Figure 4 shows two on-shore locations where time series have been extracted from the model. These are the locations where video footage from the event is available as described in Section 2.3.4. The corresponding time series are shown in Figure 12.

The estimated depths and flow rates given in Section 2.3.4 are shown together with the modelled depths and flow rates obtained from the model in Table 1. The predicted maximum depths and speeds are all of the same order of what was observed as is the approximate arrival time at the two locations. However, unlike the real event, the model estimates complete withdrawal of the water between waves at the chosen locations and shows that the model must be used with caution at this level of detail. Nonetheless, this comparison serves to check that the peak depths and speeds predicted are within the range of what is expected.

Given the uncertainties in both model and observations, there is good agreement between the values obtained from the videos and the simulations.

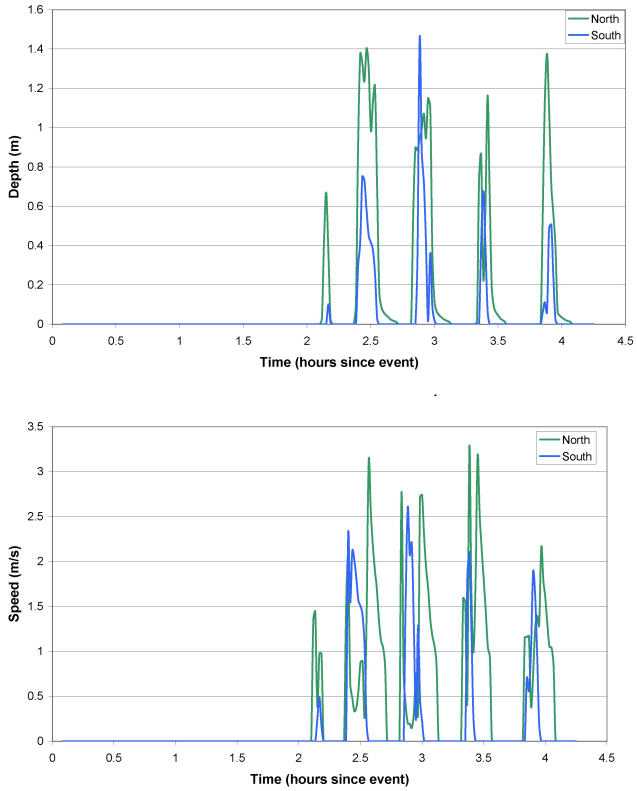

Fig. 12 Time series obtained from the two onshore locations, North and South, shown in Figure 4. Time is given in hours since the earthquake event (7:59).

	Depth [m]		Flow [m/s]	
	Observed	Modelled (peak)	Observed	Modelled (peak)
North	1.5 – 2	1.4	5 – 7	3.3
South	1.5 – 2	1.5	0.5 – 2	2.6

Table 1 Observed depth and flows from the video footage compared to values extracted from the inundation model.

5 Sensitivity Analysis

The numerical models used to simulate tsunami impact are computationally intensive and high resolution models of the entire evolution process will often take a number of days to compute. Consequently, the uncertainty in model predictions is difficult to quantify as it would require a very large number of runs. However, model uncertainty should not be ignored. The aim of this section is not to provide a detailed investigation of sensitivity but to rather illustrate that changes in important parameters produce behaviour consistent with

the known physics and that small changes in these parameters produce bounded variations in the output.

This section investigates the effect of different values of Manning's friction coefficient, changing wave height at the 100 m depth contour, and the presence and absence of buildings in the elevation dataset on model maximum inundation as computed by ANUGA.

The reference model is the one reported in Figure 10 (right) with a friction coefficient of 0.01, buildings included and the boundary condition produced by the URSGA model.

5.1 Friction

The first sensitivity study investigated the impact of surface roughness on the predicted run-up. According to Schoettle [22] appropriate values of Manning's coefficient range from 0.007 to 0.03 for tsunami propagation over a sandy sea floor and the reference model uses a value of 0.01. To investigate sensitivity to this parameter, we simulated the maximum on-shore inundation using a Manning's coefficient of 0.0003 and 0.03. The resulting inundation maps are shown in Figure 14 and the maximum flow speeds in Figure 15. The figure, along with Table 2, shows, as expected, that the on-shore inundation extent decreases with increasing friction and that small perturbations in the friction cause bounded changes in the output. This is consistent with the conclusions of Synolakis [25] et al, who state that the long wavelength of tsunami tends to mean that friction is less important in comparison to the motion of the wave.

5.2 Input Wave Height

Wave heights in the open ocean are generally well predicted by the generation and propagation models such as URSGA as demonstrated in Section 4.2 and also in [28] assuming that the source parameters are chosen appropriately[4]. Nevertheless, the effect of errors in the wave height used as input to ANUGA was investigated by perturbing the amplitude of the input wave by ± 10 cm. This value was chosen somewhat arbitrarily to be roughly consistent with the expected error in the amplitude of the leading wave as predicted by the propagation model and amounts to about $\pm 5\%$ of the maximal wave height at the boundary between the two models.

Figure 16, Figure 17 and Table 2 indicate that the inundation severity is directly proportional to the boundary wave height but small perturbations in the input wave height of 10 cm appear to have little effect on the final inundated area. Obviously larger perturbations would have greater impact.

5.3 Buildings and Other Structures

The presence or absence of physical buildings in the elevation model was also investigated as shown in Figure 18. From Table 2 it is apparent that densely built-up areas act as dissipators greatly reducing the inundated area. Figure 19 shows the associated flow speeds in the presence and absence of buildings (bare earth). It is evident that flow speeds tend to increase in passages between buildings but slow down in areas behind them as compared to

[4] As the estimates of the Sumatra-Andaman earthquake vary from magnitude 9.1 to 9.3, uncertainties in the source parameters can be considerable.

	ρ_{in}	ρ_{out}
Reference model	0.79	0.20
Friction = 0.0003	0.83	0.26
Friction = 0.03	0.67	0.09
Boundary wave height minus 10 cm	0.77	0.17
Boundary wave height plus 10 cm	0.82	0.22
No Buildings	0.94	0.44

Table 2 ρ_{in} and ρ_{out} of the reference simulation and all sensitivity studies.

the bare earth scenario. These results suggest that, when possible, the presence of human-made structures should be included into the model topography. Furthermore, these results also indicate that simply matching point sites with much lower resolution meshes or, indeed, areas of artificially high friction than used here is an over simplification. Such simulations cannot capture the fine detail that so clearly affects inundation depth and flow speeds.

6 Conclusion

This paper proposes a new field data benchmark for the validation of tsunami inundation models. Currently, there is a scarcity of appropriate validation datasets due to a lack of well-documented historical tsunami impacts. The benchmark proposed here utilises the uniquely large amount of observational data for model comparison obtained during, and immediately following, the Sumatra–Andaman tsunami of 26 December 2004. The proposed benchmark is intended to aid validation of tsunami inundation, which is the most important stage of tsunami evolution. However individual tests are presented to facilitate model evaluation for the generation and propagation phases as well. In an attempt to provide higher visibility and easier accessibility for tsunami benchmark problems, the data used to construct the proposed benchmark is documented and freely available at `http://tinyurl.com/patong2004-data`.

An associated aim of this paper was to further validate the URSGA–ANUGA tsunami modelling methodology employed by Geoscience Australia which is used to simulate tsunami inundation. This study shows that the tsunami modelling methodology adopted is credible and able to predict detailed inundation extents and dynamics with reasonable accuracy. Model predictions matched well a detailed inundation survey of Patong City as well as altimetry data from the JASON satellite, eye-witness accounts of wave front arrival times and onshore flow speeds.

A simple sensitivity analysis was performed to assess the influence of small changes in friction, wave height at the 100 m depth contour and the presence of buildings on the model predictions. Of these three, the presence of buildings was shown to have the greatest influence on the simulated inundation extent. This result indicates that the influence of human-made structures should be included, where possible, in any future studies. The value of friction and small perturbations in the wave height at the ANUGA boundary have comparatively little effect on the model results.

Acknowledgements This project was undertaken at Geoscience Australia and the Department of Mathematics, The Australian National University. The authors would like to thank Niran Chaimanee from the CCOP for providing the post 2004 tsunami survey data, building footprints, satellite image and the elevation data for Patong city; Prapasri Asawakun from the Suranaree University of Technology and Parida Kuneepong for supporting this work; Drew Whitehouse from the Australian National University for preparing the animation of

the simulated impact; and Rick von Feldt for locating the Novotel from the video footage and for commenting on the model from and eye-witness point of view.

This paper is published with the permission of the Chief Executive Officer, Geoscience Australia.

7 Appendix

This appendix present the images used to assess the model sensitivities described in Section 5.

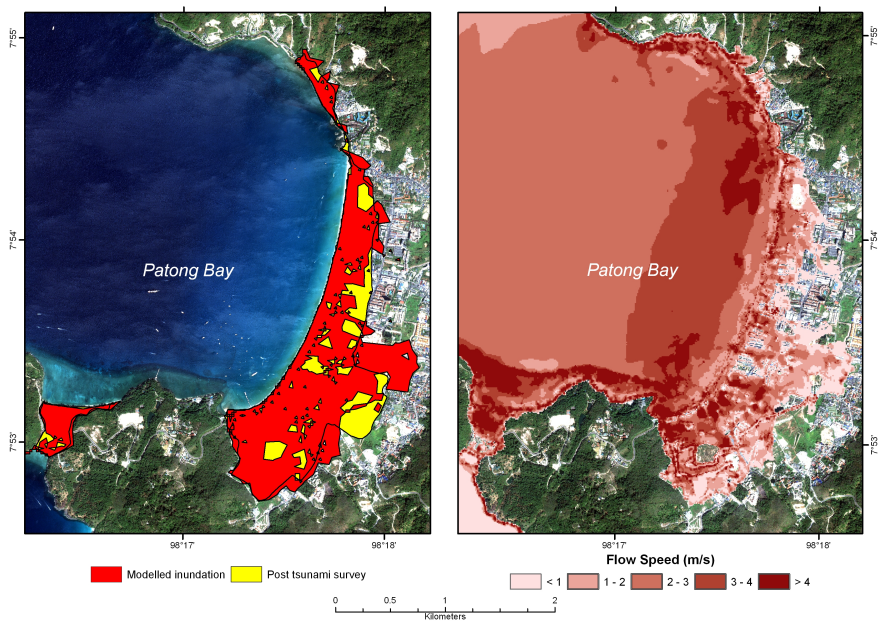

Fig. 13 Results from reference model as reported in Section 4, i.e. including buildings and a friction value of 0.01. The seaward boundary condition is as provided by the URSGA model. The left image shows the maximum modelled depth while the right hand image shows the maximum modelled flow speeds.

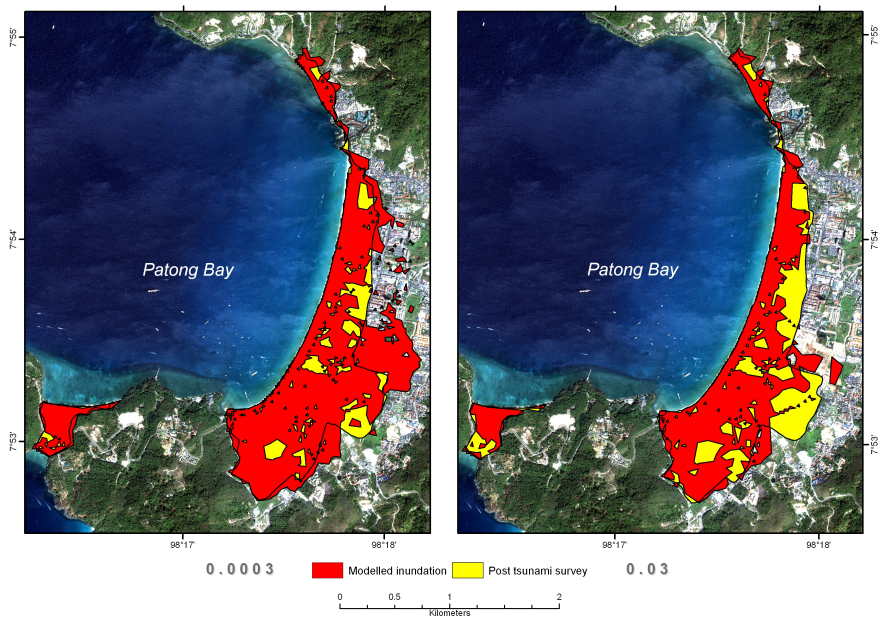

Fig. 14 Model results for different values of Manning's friction coefficient shown to assess sensitivities. The reference inundation extent for a friction value of 0.01 is shown in Figure 13 (left). The left and right images show the inundation results for friction values of 0.0003 and 0.03 respectively. The inundation extent increases for the lower friction value while the higher slows the flow and decreases the inundation extent. Ideally, friction should vary across the entire domain depending on terrain and vegetation. This, however, is beyond the scope of this study.

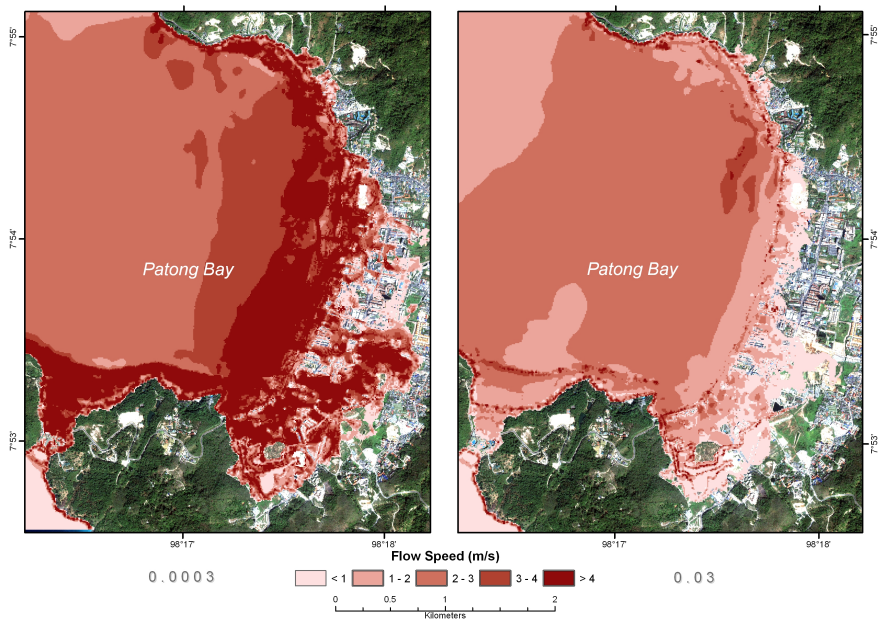

Fig. 15 The maximal modelled flow speeds for the same model parameterisations found in Figure 14. The reference flow speeds for a friction value of 0.01 are shown in Figure 13 (right).

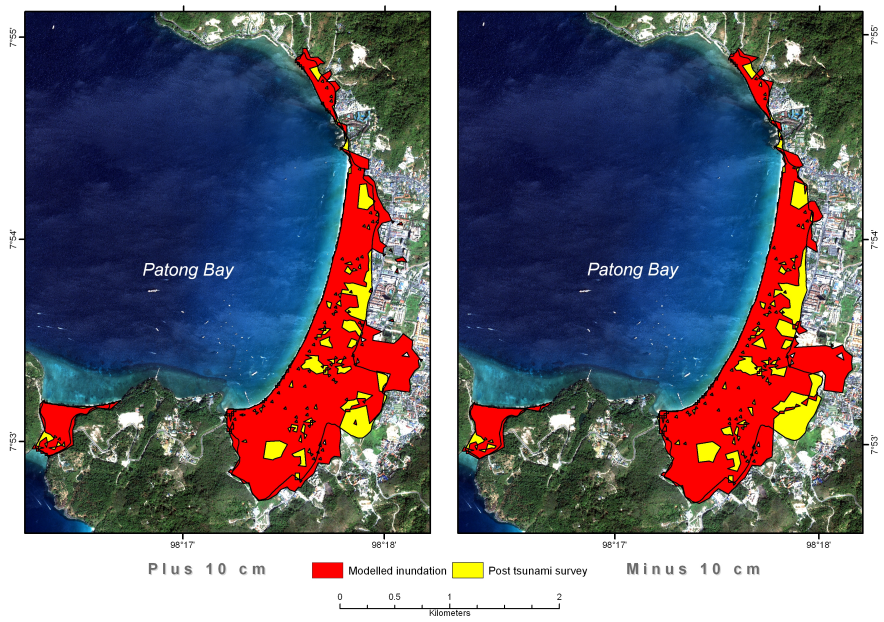

Fig. 16 Model results with wave height at ANUGA boundary artificially modified to assess sensitivities. The reference inundation extent is shown in Figure 13 (left). The left and right images show the inundation results if the wave at the ANUGA boundary is increased or reduced by 10 cm respectively. The inundation severity varies in proportion to the boundary wave height, but the model results are only slightly sensitive to this parameter for the range of values tested.

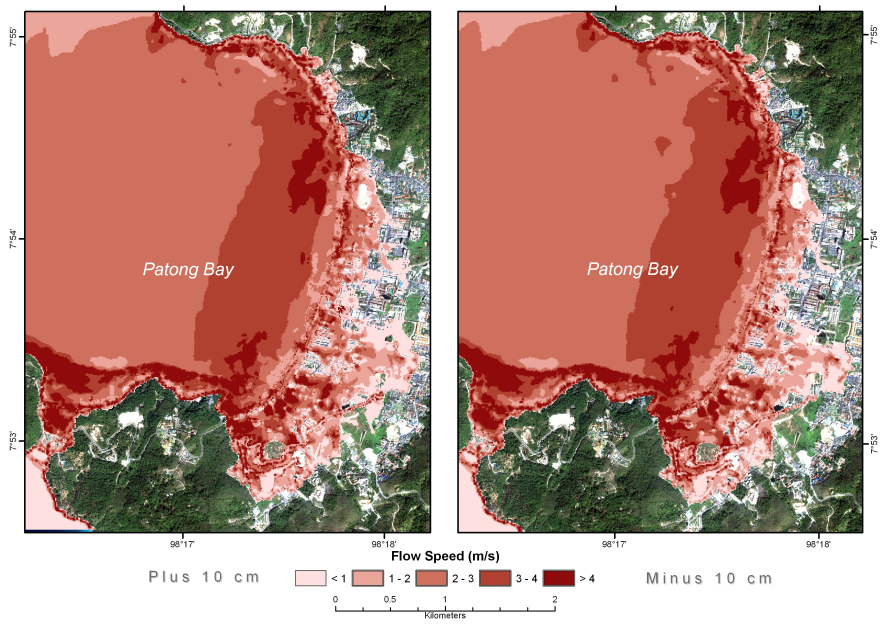

Fig. 17 The maximal flow speeds for the same model parameterisations found in Figure 16. The reference flow speeds are shown in Figure 13 (right).

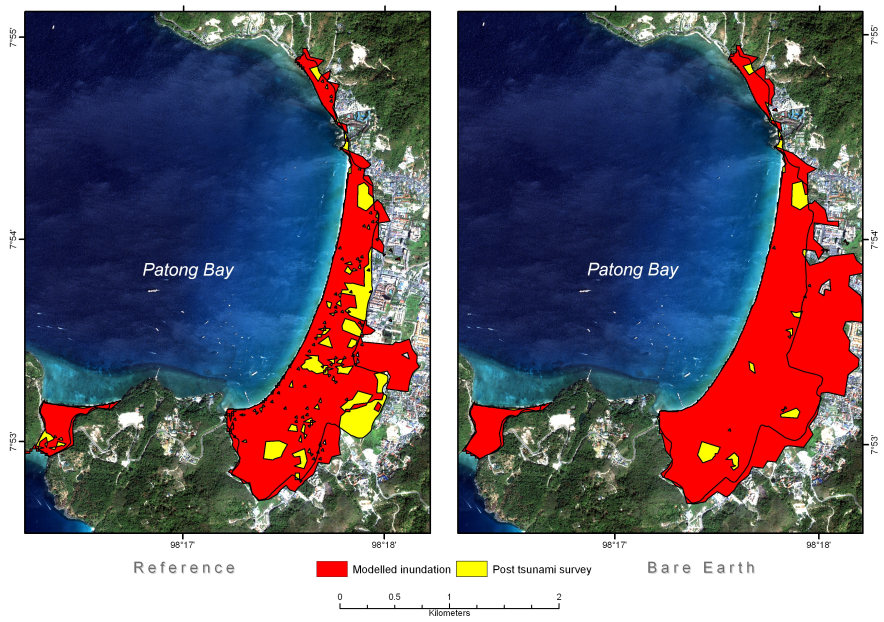

Fig. 18 Model results show the effect of buildings in the elevation data set. The left hand image shows the inundation extent as modelled in the reference model (Figure 13, left) which includes buildings in the elevation data. The right hand image shows the result for a bare earth model i.e. entirely without buildings. As expected, the absence of buildings will increase the inundation extent beyond what was surveyed.

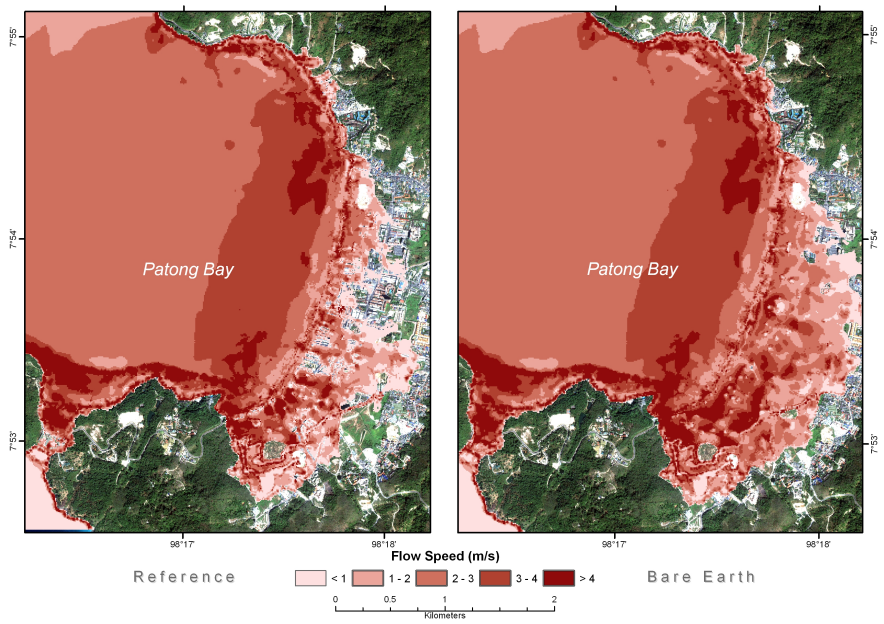

Fig. 19 The maximal flow speeds for the same model parameterisations found in Figure 18. As expected the presence of buildings reduce the flow speeds behind them, but tends to increase speeds in passages between buildings.

References

1. Ammon, C., Ji, C., Thio, H., Robinson, D., Ni, S., Hjorleifsdottir, V., Lay, H., T., L., Das, S., Helmberger, D., Ichinose, G., Polet, J., Wald, D.: Rupture Process of the 2004 Sumatra-Andaman Earthquake. Science **308** (2005)
2. Arcas, R., Titov, V.V.: Sumatra Tsunami: Lessons From Modelling. Surveys in Geopyhics **27**(6), 679–705 (2006)
3. Asavanant, J., Ioualalen, M., Kaewbanjak, N., Grilli, S.T., Watts, P., Kirby, J.T., Shi, F.: Modeling, Simulation and Optimization of Complex Processes, chap. Numerical Simulation of the December 26, 2004: Indian Ocean Tsunami, pp. 59–68. Springer Berlin Heidelberg (2008)
4. Baldock, T.E., Morrison, N., Shimamoto, T., Barnes, M.P., Gray, D., Nielsen, O.: Application and Testing of the ANUGA Tsunami Model for Overtopping and Coastal Sediment Transport. Coasts and Ports (2007). URL `http://espace.library.uq.edu.au/view/UQ:162408`
5. Bates, P., Anderson, M.: Model Validation: Perspectives in Hydrological Science, chap. Validation of hydraulic models, pp. 325–356. John Wiley and Sons, Ltd. (2001)
6. Burbidge, D., Cummins, P., Mleczko, R., Thio, H.: A Probabilistic Tsunami Hazard Assessment for Western Australia. Pure Appl. Geophys. **165**, 2059–2088 (2008). `http://dx.doi.org/10.1007/s00024-008-0421-x`
7. Chlieh, M., Avouac, J.P., Hjorleifsdottir, V., Song, T.H.A., Ji, C., Sieh, K., Sladen, A., Herbert, H., Prawirodirdjo, L., Bock, Y., Galetzka, J.: Coseismic slip and afterslip of the great M_W 9.15 Sumatra-Andaman Earthquake of 2004. Bulletin of the Seismological Soceity of America **97**(1A), S152–S173 (2007). `http://dx.doi.org/10.1785/0120050631`
8. Fritz, H.M., Borrero, J.C., Synolakis, C.E., Yoo., J.: 2004 Indian Ocean tsunami flow velocity measurements from survivor videos. Geophys. Res. Lett. **L24605**, 1–5 (2006)
9. George, D., LeVeque, R.: Finite Volume Methods and Adaptive Refinement for Global Tsunami Propagation and Indundation. Science of Tsunami Hazards **24**(5), 319–328 (2006)
10. Gower, J.: Jason 1 detects the 26 December 2004 tsunami. EOS **86**(4), 37–38 (2005)
11. Grilli, S., Ioualalen, M., Asavanant, J., Shi, F., Kirby, J., Watts, P.: Source Constraints and Model Simulation of the December 26, 2004, Indian Ocean Tsunami. Journal of Waterway, Port, Coastal, and Ocean Engineering **133**(6), 414–428 (2007). `http://dx.doi.org/10.1061/(ASCE)0733-950X(2007)133:6(414)`. URL `http://link.aip.org/link/?QWW/133/414/1`
12. Ioualalen, M., Asavanant, J., Kaewbanjak, N., Grilli, S.T., Kirby, J.T., Watts, P.: Modeling the 26 December 2004 Indian Ocean tsunami: Case study of impact in Thailand. J. Geophys. Res. **112** (2007). `http://dx.doi.org/http://dx.doi.org/10.1029/2006JC003850`
13. Kurganov, A., Noelle, S., Petrova, G.: Semidiscrete central-upwind schemes for hyperbolic conservation laws and Hamilton-Jacobi equations. SIAM Journal of Scientific Computing **23**(3), 707–740 (2001)
14. Liu, Y., Shi, Y., Yuen, D., Sevre, E., Yuan, X., Xing, H.: Comparison of Linear and Nonlinear Shallow Wave Water Equations Applied to Tsunami Waves over the China Sea. Acta Geotechnica **4**(2), 129–137 (2009). `http://dx.doi.org/10.1007/s11440-008-0073-0`. URL `http://dx.doi.org/10.1007/s11440-008-0073-0`
15. Meltzner, A.J., Sieh, K., Abrams, M., Agnew, D.C., Hudnut, K.W., Avouac, J.P., Natawidjaja, D.H.: Uplift and subsidence associated with the great Aceh-Andaman earthquake of 2004. J. Geophys. Res. **111** (2006). `http://dx.doi.org/10.1029/2005JB003891`
16. Nielsen, O., Roberts, S., Gray, D., McPherson, A., Hitchman, A.: Hydrodynamic modelling of coastal inundation. In: A. Zerger, R. Argent (eds.) MODSIM 2005 International Congress on Modelling and Simulation, pp. 518–523. Modelling and Simulation Society of Australia and New Zealand (2005). `http://www.mssanz.org.au/modsim05/papers/nielsen.pdf`
17. Papadopoulos, G.A., Caputo, R., McAdoo, B., Pavlides, S., Karastathis V. Fokaefs, A., Orfanogiannaki, K., Valkaniotis, S.: The large tsunami of 26 December 2004: Field observations and eyewitnesses accounts from Sri Lanka, Maldives Is. and Thailand. Earth, Planets and Space **58**, 233–241 (2006)
18. Roberts, S., Nielsen, O., Jakeman, J.D.: Simulation of Tsunami and Flash Flood. In: International Conference on High Performance Scientific Computing: Modeling, Simulation and Optimization of Complex Processes. Hanoi, Vietnam (2006)
19. Roberts, S., Zoppou, C.: Robust and efficent solution of the 2D shallow water wave equation with domains containg dry beds. The ANZIAM Journal **42**(E), C1260–C1282 (2000)
20. Romano, M., Liong, S.Y., Vu, M., Zemskyy, V., Doan, C., Dao, M., Tkalich, P.: Artificial Neural Network for Tsunami Forecasting. Journal of Asian Earth Sciences **36**(1), 29–37 (2009). `http://dx.doi.org/DOI:10.1016/j.jseaes.2008.11.003`. URL `http://www.sciencedirect.com/science/article/B6VHG-4V35475-1/2/91dface8aa1777e5d8bcd15d8ce95a55`
21. Satake, K.: Linear and nonlinear computations of the 1992 Nicaragua earthquake tsunami. Pure and Applied Geophysics **144**(3), 455–470 (1995)

22. Schoettle, E., Sakimoto, S.: Modeling the Effects of Coral Reef Health on Tsunami Run-up with the Finite-element Model ADCIRC. http://istim.ce.nd.edu/2007/Posters/Schoettle_poster.pdf (2007). University of Notre Dame
23. Stein, S., Okal, E.: Ultralong Period Seismic Study of the December 2004 Indian Ocean Earthquake and Implications for Regional Tectonics and the Subduction Process. Bulletin of the Seismological Society of America **97**(1A), S279S295 (2007)
24. Synolakis, C., Bernard, E., Titov, V., Kanoglu, U., Gonalez, F.: Validation and Verification of Tsunami Numerical Models. Pure and Applied Geophysics **165**, 2197–2228 (2008). http://dx.doi.org/10.1007/s00024-004-0427-y
25. Synolakis, C., Okal, E., Bernard, E.: The megatsunami of December 26 2004. National Academy of Engineering Publications (2005)
26. Szczucinski, W., Chaimanee, N., Niedzielski, P., Rachlewicz, G., Saisuttichai, D., Tepsuwan, T., Lorenc, S., Siepak, J.: Environmental and geological impacts of the 26 December 2004 tsunami in coastal zone of Thailand - overview of short and long-term effects. Polish Journal of Environmental Studies **15**(5), 793–810 (2006)
27. Thio, H., Somerville, P., Inchinose, G.: Probabilistic analysis of tsunami hazards in Southeast Asia. J. Earthquakes and Tsunami **1**, 119–137 (2008)
28. Thomas, C., Burbidge, D.: A Probabilistic Tsunami Hazard Assessment of the Southwest Pacific Nations. Tech. rep., Geoscience Australia Professional Opinion No. 2009/2. GeoCat No. 68193 (2009)
29. Titov, V., Gonzalez, F.: Implementation and testing of the method of splitting tsunami (MOST) model. NOAA Technical Memorandum (1997)
30. Wang, R., Martin, F.L., Roth, F.: Computation of deformation induced by earthquakes in a multi-layered crust FORTRAN programs EDGRN/EDCMP. Comp. and Geosc. (2006)
31. Watts, P., Ioualalen, M., Grilli, S., Shi, F., Kirby, J.: Numerical Simulation of the December 26, 2004 Indian Ocean Tsunami using a Higher-order Boussinesq Model. In: Ocean Waves Measurement and Analysis 5th International Symposium (2005)
32. Weiss, R., Wunnemann, K., Bahlburg, H.: Numerical Modelling of Generation, Propagation and Runup of Tsunamis Caused by Ocean Impacts: Model Strategy and Technical Solutions. Geohpys. J. Int. **167**, 77–88 (2006). http://dx.doi.org/doi:10.1111/j.1365-246X.2006.02889.x
33. Wessel, P., Smith, W.: New, improved version of Generic Mapping Tools released. EOS trans. AGU (1998)
34. Zhang, Y., Baptista, A.: An Efficient and Robust Tsunami Model on Unstructured Grids. Part I: Inundation Benchmarks. Pure and Applied Geophysics **165**(11), 2229–2248 (2008). http://dx.doi.org/10.1007/s00024-008-0424-7. URL http://www.springerlink.com/content/h041546220105441
35. Zoppou, C., Roberts, S.: Catastrophic collapse of water supply reservoirs in urban areas. Journal of Hydraulic Engineering **125**(7), 686–695 (1999)
36. Zoppou, C., Roberts, S.: Numerical solution of the two-dimensional unsteady dam break. Applied Mathematical Modelling **24**, 457–475 (2000)